Reaction pathway of oxygen evolution on Pt(111) revealed through constant Fermi level molecular dynamics

Assil Bouzid*, Patrick Gono, Alfredo Pasquarello

Chaire de Simulation à l'Echelle Atomique (CSEA), Ecole Polytechnique Fédérale de Lausanne (EPFL), CH-1015 Lausanne, Switzerland

Abstract

The pathway of the oxygen evolution reaction at the Pt(111)/water interface is disclosed through constant Fermi level molecular dynamics. Upon the application of a positive bias potential H_2O_{ads} and OH_{ads} adsorbates are found to arrange in a hexagonal lattice with an irregular alternation. Increasing further the electrode potential then induces the oxygen evolution reaction, which is found to proceed through a hydrogen peroxide intermediate. Calculation of the associated overpotential shows a reduction of 0.2 eV compared to the associative mechanism. This result highlights the forcefullness of the applied scheme in exploring catalytic reactions in an unbiased way.

Keywords:

OER mechanism, molecular dynamics, constant Fermi level molecular dynamics

Reducing CO_2 emissions is becoming a worldwide necessity in order to limit the impact of global warming. This requires developing new energy sources that go beyond internal combustion engines [1, 2, 3]. Alkaline and proton-exchange-membrane fuel cells are among the most promising alternatives thanks to their high energy efficiency [1, 2, 3]. Enhancing the performance of fuel cells requires a catalyst that can efficiently catalyze the hydrogen and oxygen evolution at the same time. While platinum remains the best electrocatalyst for fuel cells [4], many efforts focus on developing efficient and low-cost electrode materials. At this level, a thorough understanding of the oxygen evolution reaction (OER) mechanism under realistic conditions is instrumental for further progress.

The reverse reaction, the oxygen reduction reaction, is generally assumed to evolve through four proton-coupled electrons transfers according to an associative mechanism [5]. The pathway of the OER can then be inferred under the assumption that the same intermediates occur. In

*Corresponding author

Email address: assil.bouzid@unilim.fr (Assil Bouzid)

alcaline conditions, this gives:

$$^* + H_2O \rightarrow OH_{ads} + (H^+ + e^-),$$
$$OH_{ads} \rightarrow O_{ads} + (H^+ + e^-),$$
$$O_{ads} + H_2O \rightarrow OOH_{ads} + (H^+ + e^-),$$
$$OOH_{ads} \rightarrow O_{2g} + (H^+ + e^-),$$

where the asterisk indicates an active surface site. First, water molecules dissociate leading to hydroxyl ions adsorbed at the metal surface and hydronium ions in the aqueous solution. Second, OH_{ads} releases a proton and forms an adsorbed O. Third, OOH_{ads} forms upon the next proton-coupled electron transfer. Finally, an oxygen molecule is formed and released from the metal surface. The high stability of the intermediate step with O_{ads} is assumed to determine the overpotential of the overall reaction [5].

In the OER pathway given above, the detailed role of intermediate adsorbates, such as OH_{ads}, remains elusive. On the one hand, it has been shown that OH_{ads} slows down the kinetics of the OER by blocking the catalytically active sites [6, 7]. On the other hand, it facilitates the reaction by stabilizing H_2O_{ads} through the formation of hydrogen bonds [8, 9, 10]. The reaction could further complexify through the formation of a hydrogen peroxide (H_2O_{2ads}) intermediate as proposed by Wroblowa *et al.* [11] and supported by several experimental observations [12, 13, 14, 15, 16, 17, 18, 19, 20].

While assessing the OER mechanism from experiments remains difficult [21], density functional theory (DFT) can provide valuable and detailed insights into the reaction pathways and their energetics [5, 22, 10, 23, 24, 25]. However, current modeling techniques in which the number of electrons remains constant do not provide direct access to the reaction mechanisms, and rely on a prior knowledge of the reaction intermediates. It is therefore highly desirable to implement modeling schemes that allow chemical reactions to take place spontaneously at finite temperature and under bias potential [26, 27, 28, 29, 30, 31]. Such techniques would make possible the exploration of intermediate species and the investigation of their role in the OER as a function of the applied potential in a dynamically unconstrained fashion [27].

In this Communication, we explore the use of constant Fermi level molecular dynamics [32, 27] to investigate electron-transfer reactions at metal-water interfaces under bias potential, focusing in particular on the OER at Pt(111) electrodes. We pursue the following two-step strategy. First, we use constant Fermi level molecular dynamics to allow the system to evolve spontaneously without taking advantage of any previous knowledge that could bias the outcome of the simulation. Accordingly, we study the Pt surface coverage under positive bias potential and discuss the spontaneous arrangement of the adsorbates. By further increasing the applied potential, we then induce

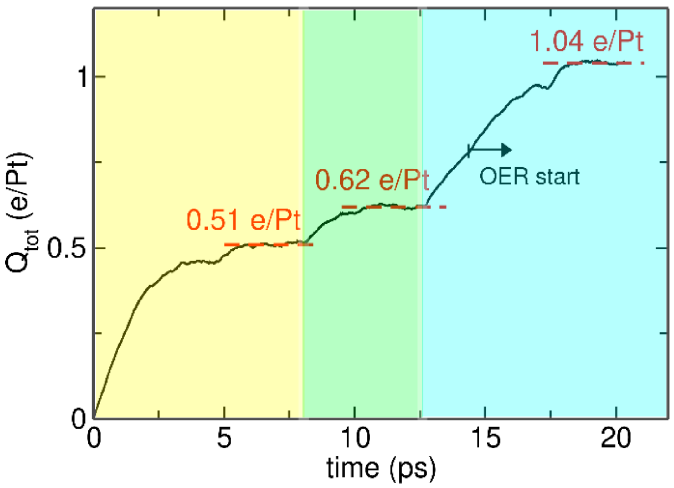

Figure 1: Time evolution of the excess electronic charge Q_{tot} in constant Fermi level molecular dynamics of the Pt(111)/water interface. Q_{tot} is given per number of Pt atoms. The background colors indicate three different potential regimes.

the OER at the Pt surface and explore the pathway freely undertaken by the system. Next, we determine the free energies of the identified intermediates within a conventional scheme, namely the computational standard hydrogen electrode, in order to examine whether the revealed pathway is viable.

In constant Fermi level molecular dynamics, the Fermi level is maintained at a preset fixed value during the evolution and is therefore particularly suited for simulating the effect of the bias potential in the simulation of electrified metal-water interfaces [32, 27]. This is achieved through the introduction of grand canonical potential, by which the charge can flow in and out of the system so that the condition on the Fermi level is satisfied. In practice, the electronic charge in the system is treated like a classical variable with inertia and is subject to fictitious dynamical equations. To ensure a good control over the potential fluctuations, it is also possible to couple the physical system to a thermostat ensuring a tempurature T, while keeping the electron reservoir at a temperature T_e [32]. The use of two different thermostats does not create any significant thermal flow in the system due to the weak coupling between atoms and charges [32]. When applying constant Fermi level simulations to reactions occurring at metal-water interfaces, it should be kept in mind that this corresponds to the modeling of a rare event with a computational setup of relatively small size and on time scales that can be reached with molecular dynamics techniques. In the present approach, the intrinsic barriers associated to these events are overcome by increasing the bias potential until the reaction is seen to proceed spontaneously. While enforcing the reaction in this way appears sufficient to reveal interesting reaction pathways in this work, it could be envisaged to combine the present constant Fermi level molecular dynamics with more sophisticated approaches for treating rare events, such as metadynamics, Blue Moon, or umbrella sampling techniques.

We adopt the periodic Pt(111)/water interface model generated in Ref. 27, in which a Pt slab shows two equivalent interfaces with the water layer, denoted surface 1 and surface 2. The su-

percell contains three Pt layers of 12 atoms with a $3\times\sqrt{3}$ surface repeat unit and 32 water molecules, corresponding to a size of $9.79\times8.48\times19.50$ Å^3. While the finite size of the water layer containing 32 water molecules only approximately accounts for the properties of liquid water at the interface, the O-O pair correlation function and the water density in the middle of the slab are in fair agreement with the corresponding properties of bulk water [27]. Furthermore, the dipoles of the water molecules remain randomly oriented even under bias potential. Therefore, in view of the fact that we focus in this work on electrochemical processes occurring at the metal-water interface, we assume that the finite size of the water layer only induces a limited bias in identifying the relevant reaction pathways. Furthermore, the adopted simulation cell combined with the use of a uniform compensating background charge yields the advantage that the electric field is realistically modelled at the Pt/water interface (*vide infra*) [27]. In any event, we remark that our strategy comprises an a posteriori validation of the identified intermediate steps within a conventional state-of-the-art scheme.

The constant Fermi level molecular dynamics [27, 33, 34, 26] in this work relies on a description of the electronic structure within density functional theory (DFT) through an optimized rVV10 functional [35, 36, 37]. In the rVV10 functional used in this work, the b parameter is set to 9.3 to ensure a good description of the water density [37]. Core-valence interactions are treated through normconserving pseudopotentials [38] and the wave functions of the valence electrons are expanded on a plane-wave basis set defined by a kinetic-energy cutoff of 80 Ry. The Brillouin zone is sampled at the Γ point. Constant Fermi level molecular dynamics simulations at $T = 350$ K are performed within the Born-Oppenheimer scheme with a time step of $\Delta t = 0.48$ fs to integrate the equations of motion, as implemented in the Quantum-ESPRESSO suite of programs [39]. Temperature control is ensured through velocity rescaling. In the constant Fermi level scheme, the mass of the fictitious charge degrees of freedom is set to $M_\mathrm{e} = 100$ a.u. The fictitious electronic temperature is controlled by a velocity rescaling method and is set to $T_\mathrm{e} = 30$ K. Gaussian-smeared occupations with widths of at most 0.10 eV are used to prevent numerical instabilities [27, 33, 34, 26]. In the present dynamics, the inertial mass is set in such a way that the fluctuations of the grand canonical potential occur on a time scale that accompanies the structural rearrangements, to account for smooth transitions upon charge variations in the physical system. While this choice affects the time scales over which equilibrium is reached, the final state and its energetics are only determined by the grand-canonical potential.

When modeling a heterogeneous system con-

sisting of an electrode-water system, a further issue arises concerning the compensation of the electron charge on the electrode. Taylor et al. proposed a scheme based on a uniform background charge to compensate the electron charge injected in the system [40]. Applying an alignment procedure through a vacuum layer placed in the middle of the water layer allowed them to reference the electrode potential to the vacuum level. In our approach, we also resort to a uniform background to ensure the overall neutrality of the simulation cell. However, we correct the charge and electrode potential through classical electrostatics and introduce an intrinsic alignment scheme based on the computational standard hydrogen electrode to reference the electrode potential [27]. It has been shown in Ref. 27 that, for specific sizes of the simulation cell, the profile of the electric field across the interface closely resembles that of the physical interface in which the electrode charge is compensated by a distribution of counterions. Hence, such an electrode model provides a convenient tool for investigating electrified metal-water interfaces. More details about the computational setup and the model are provided in the Supporting Information of Ref. 27.

We note that the use of a neutralizing background does not solve the general problem of modelling electrified interfaces from first principles. When modelling a half cell, one of the main difficulties consists in adapting the counter charge of the electrolyte as the electrode potential is varied. This implies inserting extra ionic charges into the electrolyte under conditions pertaining to a grand-canonical modelling scheme. When considering the results obtained with the more approximate scheme used in this work, it should therefore be borne in mind that it is at present unknown to what extent the description of the alignments and of the reaction mechanisms might be altered when treating the counterions in such an atomistic way.

Starting from a neutral system, we increment the bias potential towards positive values on the conventional scale referred to the standard hydrogen electrode. In order to define the surface bias properly in our simulation it is necessary to determine the potential of the electrode with respect to the electrostatic potential in liquid water. However, as the reaction proceeds in the simulation, a large number of protons are injected in the water layer preventing us from recovering the potential of pure liquid water. Hereafter, we therefore characterize the Pt(111)/water system by the total electronic charge as this quantity is directly related to the applied potential [27]. To model increasing bias potentials, the total electronic charge goes through three plateaus as a function of simulation time, being incremented by a discrete amount from one value to the next [27]. Anytime the charge is varied, the system recovers equilibrium in a few picoseconds, as shown in Fig. 1. This time period ensures that the system

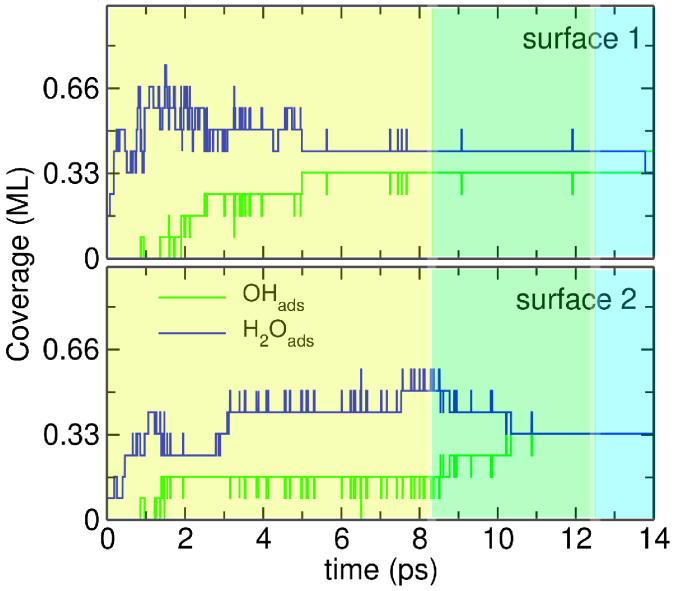

Figure 2: Time evolution of the H_2O_{ads} and OH_{ads} surface coverage on the two individual surfaces in our model, surface 1 (top) and surface 2 (bottom). The background colors indicate the three potential regimes.

accommodates the injected electronic charge and that the water molecules arrange their structure accordingly.

During the first part of the dynamics ($t < 8$ ps) at a potential corresponding to 0.51 e^-/Pt (see Fig. 2), part of the water molecules dissociate leading to the formation of adsorbed hydroxyl ions (OH_{ads}) at the Pt surface and to the injection of hydronium ions (H_3O^+) into the water layer, as shown in Fig. 3. We remark that despite the increase in acidity of the water layer, the surface coverage stabilized by the bias potential shows a high percentage of hydroxyls, typical of alcaline conditions. As the electronic charge is increased further to 0.62 e^-/Pt ($8 < t < 12$ ps), the number of adsorbed species at the Pt surface reaches equilibrium. During the last part of the dynamics and before the OER takes place, only a few proton transfers between OH_{ads} and H_2O_{ads} are observed at the Pt surface. We find that the equilibrated surface structure corresponds to an OH_{ads} coverage of 1/3 monolayer (ML). In addition, the H_2O_{ads} coverage at equilibrium is found to be equal to 5/12 ML at surface 1 and 1/3 ML at surface 2. The slightly higher coverage of surface 1 is due to the adsorption of one extra water molecule at the Pt surface, indicated by an arrow in Fig. 3. Overall, the OH_{ads} coverage of 1/3 ML found through constant Fermi level molecular dynamics agrees with that predicted by static DFT calculations [22, 41, 10, 8, 9].

The elusive role of adsorbates in the OER mechanism [6, 7, 8, 9, 10] calls for a deeper understanding of their structural organization at the Pt active sites. As shown in Fig. 3, the adsorbates arrange in a honeycomb lattice, in agreement with previous predictions based on static calculations without bias potential and with a single monolayer [22, 41, 10, 8, 9]. However, H_2O_{ads} and OH_{ads} do not respect the perfect alternation as reported previously [22, 41, 10, 8, 9]. Hence, it appears that irregular surface coverages can occur under the globally different conditions of our simulation, which include the effects of finite temperature, bias potential and the interaction with water molecules beyond the first monolayer.

Next, we induce the OER by further increas-

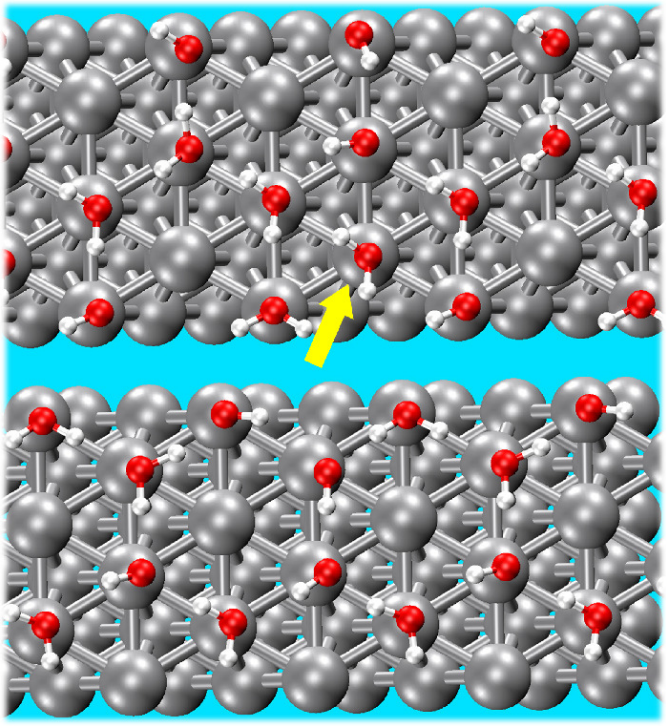

Figure 3: Representative snapshots of Pt surface 1 (top) and Pt surface 2 (bottom) at equilibrium with Q_{tot}=0.62 e^-/Pt (t=13 ps). The arrow indicates an extra water molecule adsorbed out of the hexagonal lattice.

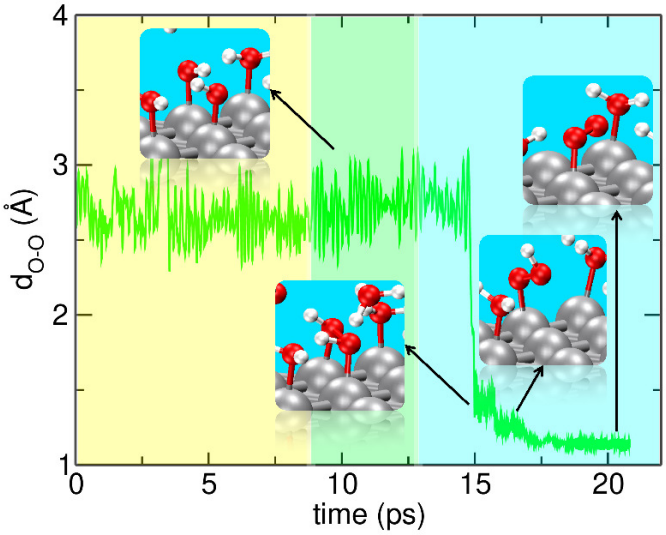

Figure 4: Time evolution of the distance between the two O atoms involved in the OER. Representative snapshots of the intermediate adsorbates are provided in the insets. The background colors indicate the three potential regimes.

ing the bias potential and focus on the reaction mechanism. As shown in Fig. 1, more electronic charge is extracted from the cell and the system is driven out of the equilibrium at Q_{tot}=0.62 e^-/Pt reaching a new state at Q_{tot}=1.04 e^-/Pt. During this transition, we observe the OER starting on surface 2 at 14.3 ps and leading to the formation of an adsorbed O_2 molecule within a few picoseconds. The OER is found to proceed through the following steps. At first, two hydroxyl ions are adsorbed at adjacent Pt active sites. Figure 4 shows the time evolution of the distance $d_{\mathrm{O-O}}$ between the oxygen atoms of the adsorbed hydroxyl ions. The distance between the two OH_{ads} fluctuates around 2.7 Å, close to the Pt-Pt distance of 2.83 Å. Second, $d_{\mathrm{O-O}}$ shortens to 1.42 Å upon the formation of a $H_2O_{2\mathrm{ads}}$ molecule. Third, $H_2O_{2\mathrm{ads}}$ releases one hydrogen and transforms into OOH_{ads}, with $d_{\mathrm{O-O}} \cong 1.25$ Å. Finally, the second hydrogen is released and the resulting $O_{2\mathrm{ads}}$ shows a $d_{\mathrm{O-O}}$ distance of 1.13 Å. This distance is very close to the equilibrium distance of 1.20 Å of gaseous O_2. Snapshots of the successive intermediate adsorbates are given in the insets of Fig. 4.

During the dynamics, we simultaneously observe the first steps of the associative mechanism up to the formation of O_{ads}, but the subsequent steps of this mechanism do not occur on the time scale of our simulation. From the observed evo-

lution, we thus draw the following mechanism for the OER on Pt:

$$^* + \mathrm{H_2O} \rightarrow \mathrm{OH_{ads}} + (\mathrm{H^+} + e^-),$$
$$\mathrm{OH_{ads}} + ^* + \mathrm{H_2O} \rightarrow 2\mathrm{OH_{ads}} + (\mathrm{H^+} + e^-),$$
$$2\mathrm{OH_{ads}} \rightarrow \mathrm{H_2O_{2ads}} \rightarrow \mathrm{OOH_{ads}} + (\mathrm{H^+} + e^-),$$
$$\mathrm{OOH_{ads}} \rightarrow \mathrm{O_{2g}} + (\mathrm{H^+} + e^-),$$

where the second step involves the adsorption of the second $\mathrm{OH_{ads}}$ in the immediate vicinity of the $\mathrm{OH_{ads}}$ adsorbed in the first step. The formation of the $\mathrm{H_2O_{2ads}}$ molecule occurs as an intermediate in the third step and is facilitated by the irregular $\mathrm{H_2O_{ads}}/\mathrm{OH_{ads}}$ hexagonal ML at the Pt surface, which allows for adjacent $\mathrm{OH_{ads}}$. We remark that the present mechanism does not rely on the formation of an $\mathrm{O_{ads}}$ intermediate. At variance, our work provides evidence for the occurrence of the hydrogen peroxide intermediate, as suggested by Wroblowa et al.[11] and supports the experimental observation of this species during the OER [12, 13, 14, 15, 16, 17, 18, 19, 20].

The pathway revealed by the constant Fermi level molecular dynamics has been enforced by driving the potential to values for which the reaction could evolve spontaneously. Furthermore, our observation hinges on a single molecular dynamics trajectory. To corroborate our finding, it is therefore necessary to critically examine the identified reaction path by resorting to a method corresponding to the state of the art. We are not aware of any generally accepted scheme to

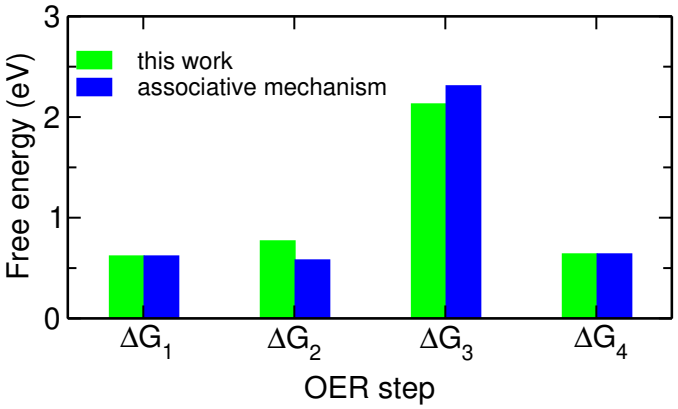

Figure 5: Gibbs free energy steps corresponding to the intermediates of the OER on Pt(111).

date involving bias potentials and explicit water that produces reliable free energies. We therefore resort to the widely used computational hydrogen electrode scheme [5]. Within this scheme, we calculate the Gibbs free energies, ΔG_1 to ΔG_4, corresponding to the four proton-coupled electron transfers. The calculations are performed at the bare Pt(111) and the systems with the intermediate adsorbates are fully relaxed at the rVV10 level of theory. To enable a meaningful comparison of the calculated free energies with those of the associative mechanism in the literature [5, 42], we here use the CP2K code [43], in which the orbitals are described with an atom-centered Gaussian-type basis set and the electron density is expanded on an auxiliary plane-wave basis set. We use triple-ζ MOLOPT basis sets [44] for all elements. The plane-wave energy cutoff is set to 800 Ry and the Brillouin zone is sampled at the Γ point. Goedecker-Teter-Hutter pseudopotentials are used to describe core-valence interac-

tions [45]. A detailed description of the adopted formulation is provided in the Supporting Information of Ref. 42.

The calculated free energies are illustrated in Fig. 5. The presently identified mechanism differs from the associative one only in the second and third steps because of the different intermediates involved. In particular, the associative mechanism involves O_{ads}, which interacts strongly with the Pt electrode leading to a high value of ΔG_3 [5, 22]. In the presently identified pathway, the OER overpotential of the overall reaction is still determined by the third proton-coupled electron transfer (ΔG_3), but it is found to be lower by 0.18 eV. This energy gain results from the extra cost of adsorbing a second OH_{ads} in the vicinity of a previously adsorbed OH_{ads}, which leads to a corresponding increase in ΔG_2. Hence, these results indicate that the adopted simulation scheme has revealed a viable reaction pathway with competitive Gibbs free energy steps.

In summary, constant Fermi level molecular dynamics at the Pt(111)/metal interface reveal that adsorbates arrange in a honeycomb lattice at the Pt surface with an OH_{ads} coverage of 1/3 ML. We find that the H_2O_{ads} and OH_{ads} do not respect the perfect alternation at the Pt surface leading to the adsorption of OH_{ads} at adjacent Pt sites. Consequently, this opens the way to the formation of an adsorbed hydrogen peroxide molecule as an intermediate species, which facilitates the OER. Free energy calculations indicate that the pathway involving a hydrogen peroxide shows a reaction overpotential that is lower by 0.2 eV compared to the associative mechanism. These results demonstrate the powerfulness of constant Fermi level molecular dynamics as un unbiased tool for identifying low-energy pathways of catalytic electrochemical reactions.

This project has received funding from the European Union's Seventh Framework Programme for research, technological development and demonstration under grant agreement no. 291771 (call 2014). This work has been performed in the context of the National Center of Competence in Research (NCCR) "Materials' Revolution: Computational Design and Discovery of Novel Materials (MARVEL)" of the Swiss National Science Foundation. We used computational resources of CSCS, SCITAS, and CSEA-EPFL.

References

[1] G. Fontaras, Z. Samaras, A quantitative analysis of the european automakers voluntary commitment to reduce co_2 emissions from new passenger cars based on independent experimental data, Energy Pol. 35 (4) (2007) 2239–2248.

[2] S. A. Basha, K. R. Gopal, S. Jebaraj, A review on biodiesel production, combustion, emissions and performance, Renew. Sustain. Energy Rev. 13 (6-7) (2009) 1628–1634.

[3] A. Samanta, A. Zhao, G. K. Shimizu, P. Sarkar, R. Gupta, Post-combustion co_2 capture using solid sorbents: a review, Ind. Eng. Chem. Res. 51 (4) (2011) 1438–1463.

[4] K. Kinoshita, Electrochemical oxygen technology, Vol. 30, John Wiley & Sons, 1992.

[5] J. K. Nørskov, J. Rossmeisl, A. Logadottir, L. Lindqvist, J. R. Kitchin, T. Bligaard, H. Jonsson, Origin of the overpotential for oxygen reduction at a fuel-cell cathode, J. Phys. Chem. B 108 (46) (2004) 17886–17892.

[6] M. F. Li, L. W. Liao, D. F. Yuan, D. Mei, Y.-X. Chen, ph effect on oxygen reduction reaction at pt (1 1 1) electrode, Electrochim. Acta 110 (2013) 780–789.

[7] J. Roques, A. B. Anderson, V. S. Murthi, S. Mukerjee, Potential shift for oh(ads) formation on the pt skin on $pt_3co(111)$ electrodes in acid theory and experiment, J. Electrochem. Soc. 152 (6) (2005) E193–E199.

[8] A. S. Bondarenko, I. E. Stephens, H. A. Hansen, F. J. Pérez-Alonso, V. Tripkovic, T. P. Johansson, J. Rossmeisl, J. K. Nørskov, I. Chorkendorff, The pt(111)/electrolyte interface under oxygen reduction reaction conditions: an electrochemical impedance spectroscopy study, Langmuir 27 (5) (2011) 2058–2066.

[9] G. Karlberg, G. Wahnström, An interaction model for oh^+ h_2o-mixed and pure h_2o overlayers adsorbed on pt(111), J. Chem. Phys. 122 (19) (2005) 194705.

[10] S. Liu, M. G. White, P. Liu, Mechanism of oxygen reduction reaction on pt(111) in alkaline solution: Importance of chemisorbed water on surface, J. Chem. Phys. C 120 (28) (2016) 15288–15298.

[11] H. S. Wroblowa, G. Razumney, et al., Electroreduction of oxygen: a new mechanistic criterion, J. Electroanal. Chem. Interf. Elec. 69 (2) (1976) 195–201.

[12] A. Gómez-Marín, K. Schouten, M. Koper, J. Feliu, Interaction of hydrogen peroxide with a pt(111) electrode, Electrochem. Commun. 22 (2012) 153–156.

[13] J. Zhang, M. B. Vukmirovic, Y. Xu, M. Mavrikakis, R. R. Adzic, Controlling the catalytic activity of platinum-monolayer electrocatalysts for oxygen reduction with different substrates, Angew. Chem. 117 (14) (2005) 2170–2173.

[14] V. Stamenkovic, N. Markovic, P. Ross Jr, Structure-relationships in electrocatalysis: oxygen reduction and hydrogen oxidation reactions on pt(111) and pt(100) in solutions containing chloride ions, J. Electroanal. Chem. 500 (1-2) (2001) 44–51.

[15] T. Schmidt, U. Paulus, H. A. Gasteiger, R. Behm, The oxygen reduction reaction on a pt/carbon fuel cell catalyst in the presence of chloride anions, J. Electroanal. Chem. 508 (1-2) (2001) 41–47.

[16] A. Schneider, L. Colmenares, Y. Seidel, Z. Jusys, B. Wickman, B. Kasemo, R. Behm, Transport effects in the oxygen reduction reaction on nanostructured, planar glassy carbon supported pt/gc model electrodes, Phys. Chem. Chem. Phys. 10 (14) (2008) 1931–1943.

[17] Y. Seidel, A. Schneider, Z. Jusys, B. Wickman, B. Kasemo, R. Behm, Mesoscopic mass transport effects in electrocatalytic processes, Faraday Discuss. 140 (2009) 167–184.

[18] N. Marković, P. Ross Jr, Surface science studies of model fuel cell electrocatalysts, Surf. Sci. Rep. 45 (4-6) (2002) 117–229.

[19] N. Marković, H. Gasteiger, B. Grgur, P. Ross, Oxygen reduction reaction on pt(111): effects of bromide, J. Electroanal. Chem. 467 (1-2) (1999) 157–163.

[20] B. Grgur, N. Marković, P. Ross, Temperature-dependent oxygen electrochemistry on platinum low-index single crystal surfaces in acid solutions, Can. J. Chem. 75 (11) (1997) 1465–1471.

[21] J. Wang, N. Markovic, R. Adzic, Kinetic analysis of oxygen reduction on pt(111) in acid solutions: intrinsic kinetic parameters and anion adsorption effects, J. Phys. Chem. B 108 (13) (2004) 4127–4133.

[22] V. Tripković, E. Skúlason, S. Siahrostami, J. K. Nørskov, J. Rossmeisl, The oxygen reduction reaction mechanism on pt (1 1 1) from density functional

theory calculations, Electrochim. Acta 55 (27) (2010) 7975–7981.

[23] V. Tripkovic, M. E. Björketun, E. Skúlason, J. Rossmeisl, Standard hydrogen electrode and potential of zero charge in density functional calculations, Phys. Rev. B 84 (11) (2011) 115452.

[24] E. Skúlason, G. S. Karlberg, J. Rossmeisl, T. Bligaard, J. Greeley, H. Jónsson, J. K. Nørskov, Density functional theory calculations for the hydrogen evolution reaction in an electrochemical double layer on the pt(111) electrode, Phys. Chem. Chem. Phys. 9 (25) (2007) 3241–3250.

[25] J. Rossmeisl, K. Chan, R. Ahmed, V. Tripković, M. E. Björketun, ph in atomic scale simulations of electrochemical interfaces, Phys. Chem. Chem. Phys. 15 (25) (2013) 10321–10325.

[26] A. Bouzid, A. Pasquarello, Redox levels through constant fermi-level ab initio molecular dynamics, J. Chem. Theory Comput. 13 (4) (2017) 1769–1777.

[27] A. Bouzid, A. Pasquarello, Atomic-scale simulation of electrochemical processes at electrode/water interfaces under referenced bias potential, J. Phys. Chem. Lett. 9 (8) (2018) 1880–1884.

[28] M. Otani, O. Sugino, First-principles calculations of charged surfaces and interfaces: A plane-wave nonrepeated slab approach, Phys. Rev. B 73 (11) (2006) 115407.

[29] M. Otani, I. Hamada, O. Sugino, Y. Morikawa, Y. Okamoto, T. Ikeshoji, Structure of the water/platinum interface – a first principles simulation under bias potential, Phys. Chem. Chem. Phys. 10 (25) (2008) 3609–3612.

[30] M. Otani, I. Hamada, O. Sugino, Y. Morikawa, Y. Okamoto, T. Ikeshoji, Electrode dynamics from first principles, J. Phys. Soc. Jpn. 77 (2) (2008) 024802.

[31] T. Ikeshoji, T. Uchida, M. Otani, M. Osawa, First-principles molecular dynamics simulation for electrochemical hydrogen production by 4,4-bipyridine molecular catalyst on silver electrode, J. Electroanal. Chem. 800 (2017) 13–18.

[32] N. Bonnet, T. Morishita, O. Sugino, M. Otani, First-principles molecular dynamics at a constant electrode potential, Phys. Rev. Lett. 109 (26) (2012) 266101.

[33] A. Bouzid, A. Pasquarello, Electron trap states at ingaas/oxide interfaces under inversion through constant fermi-level ab initio molecular dynamics, J. Phys. Condens. Matter 29 (50) (2017) 505702.

[34] A. Bouzid, A. Pasquarello, Identification of semiconductor defects through constant-fermi-level ab initio molecular dynamics: Application to gaas, Phys. Rev. Appl. 8 (2017) 014010.

[35] O. A. Vydrov, T. Van Voorhis, Nonlocal van der waals density functional: The simpler the better, J. Chem. Phys. 133 (24) (2010) 244103.

[36] R. Sabatini, T. Gorni, S. de Gironcoli, Nonlocal van der waals density functional made simple and efficient, Phys. Rev. B 87 (4) (2013) 041108.

[37] G. Miceli, S. de Gironcoli, A. Pasquarello, Isobaric first-principles molecular dynamics of liquid water with nonlocal van der waals interactions, J. Chem. Phys. 142 (3) (2015) 034501.

[38] N. Troullier, J. L. Martins, Efficient pseudopotentials for plane-wave calculations, Phys. Rev. B 43 (3) (1991) 1993–2006. doi:10.1103/PhysRevB.43.1993.

[39] P. Giannozzi, S. Baroni, N. Bonini, M. Calandra, R. Car, C. Cavazzoni, D. Ceresoli, G. L. Chiarotti, M. Cococcioni, I. Dabo, et al., Quantum espresso: a modular and open-source software project for quantum simulations of materials, J. Phys. Condens. Matter 21 (39) (2009) 395502.

[40] C. D. Taylor, S. A. Wasileski, J.-S. Filhol, M. Neurock, First principles reaction modeling of the electrochemical interface: Consideration and calculation of a tunable surface potential from atomic and electronic structure, Phy. Rev. B 73 (16) (2006) 165402.

[41] H. A. Hansen, J. Rossmeisl, J. K. Nørskov, Surface pourbaix diagrams and oxygen reduction activity of pt, ag and ni(111) surfaces studied by dft, Phys. Chem. Chem. Phys. 10 (25) (2008) 3722–3730.

[42] P. Gono, J. Wiktor, F. Ambrosio, A. Pasquarello, Surface polarons reducing overpotentials in the oxygen evolution reaction, ACS Catal. 8 (2018) 5847–5851.

[43] J. VandeVondele, M. Krack, F. Mohamed, M. Parrinello, T. Chassaing, J. Hutter, Quickstep: Fast and accurate density functional calculations using a mixed gaussian and plane waves approach, Comput. Phys. Commun. 167 (2) (2005) 103–128.

[44] J. VandeVondele, J. Hutter, Gaussian basis sets for accurate calculations on molecular systems in gas and condensed phases, J. Chem. Phys. 127 (11) (2007) 114105.

[45] S. Goedecker, M. Teter, J. Hutter, Separable dual-space gaussian pseudopotentials, Phys. Rev. B 54 (3) (1996) 1703.